Research Article

Nisa Naima Khalid, Nabilah Afiqah Mohd Radzuan*, Abu Bakar Sulong, Farhana Mohd Foudzi, and David Hui

Adhesion behaviour of 3D printed polyamide–carbon fibre composite filament

https://doi.org/10.1515/rams-2022-0281
received July 25, 2022; accepted November 09, 2022

Abstract: Fused deposition modelling is known for its ability to customise materials at peak performance for instant use but lacks in terms of interfacial adhesion of layup sequences. Hence, the mechanism of acquiring excellent interfacial adhesion, mainly via dried-up printed sample, has been discovered, resulting in the proper bonding formation upon layers. Result reveals that the flexural strength increased by 23% under 70°C drying conditions (5 h) and the impact strength increased by 240% compared to pure polyamide. This mechanism resists the deformation growth between the layers and enhances the mechanical strength at the highest level.

Keywords: carbon fibres, adhesion, delamination, mechanical testing

1 Introduction

Nowadays, advancements in technology in automotive and other fields require the use of multiple components to produce a complex geometrical structure with good material properties that can address challenges worldwide [1]. These advancements in technology have been applied in additive manufacturing, which has replaced traditional part of manufacturing, in producing complex geometrical structures with low cost and rapid prototyping based on computer-aided design [2]. Fused deposited modelling (FDM) is one of the processes in additive manufacturing that fabricates the polymer-based composite components layer-by-layer [3]. Using polymer composite materials (nanofillers and microfillers) in FDM is often preferred by researchers because these materials possess excellent mechanical properties [4,5]. In the past studies, researchers discovered that using polymer composite materials increases ultimate tensile strength by 40% when acrylonitrile butadiene styrene/cellulose nanofibre composite is used in the FDM method [6]. The reason is that the fibre is mostly dispersed along the printing direction and bears a substantial load, resulting in increased tensile strength [7].

The results of previous studies clearly showed that using polymer composite as a material shows good performance in the FDM process. However, the mechanical performance of the samples printed using the 3D printing method declines when void formation exists during printing, resulting in delamination between the layers after printing [8]. Maqsood and Rimašauskas used continuous carbon fibre (CF)-reinforced thermoplastic composite material and have reported that delamination should be avoided when it causes sudden damage and a rapid decrease in stress values because of poor interfacial adhesion between the matrix and reinforcement [9]. Understanding the failure mechanism is vital in engineering, particularly in designing products using 3D printing [10]. Thus, investigate the issue of delamination in polymer composite during 3D printing. The productivity potential for the manufacturing sector can be increased by accelerating the printing process through 3D printing, and various products can be designed with the efficient use of materials [11]. According to past studies, the demands on selecting high-quality materials should meet the desired specifications to match with the required application and reduce the defects on the sample during printing [12].

Wickramasinghe et al. reported that delamination is one of the defects that disrupt the bond between the layers; they used polylactic acid polymer material to exhibit the breakage of the layer occurring at a 90° raster

* Corresponding author: Nabilah Afiqah Mohd Radzuan, Department of Mechanical & Manufacturing Engineering, Faculty Engineering & Built Environment, Universiti Kebangsaan Malaysia, 43600 Bangi, Selangor, Malaysia, e-mail: afiqah@ukm.edu.my
Nisa Naima Khalid, Abu Bakar Sulong, Farhana Mohd Foudzi: Department of Mechanical & Manufacturing Engineering, Faculty Engineering & Built Environment, Universiti Kebangsaan Malaysia, 43600 Bangi, Selangor, Malaysia
David Hui: Department of Mechanical, University of New Orleans, Engineering Building, EN 909, 2000, Lakeshore Drive, New Orleans, LA 70148, USA

angle [13]. The strength between the bonds is one of the crucial aspects of 3D printing because it can affect the mechanical properties and durability of the printed sample structure; hence, delamination should be avoided by choosing the appropriate material. Previous studies showed that delamination occurs when the fibre located in the laminate field does not provide reinforcement through thickness. Therefore, the composite relies on a relatively weak matrix to carry the load in a particular direction. Moreover, matrix resins are usually quite brittle. Therefore, a comprehensive investigation is conducted in the present study to address the issue of delamination using polyamide-reinforced carbon fibre (PACF) via FDM method.

2 Experimental method

2.1 Materials and PACF preparations

CF, grade CFP-7-50 in powder form (Shenzhen Yataida High-Tech. Co. Ltd, supplied by Sigma-Aldrich Sdn. Bhd., Malaysia), has an average diameter of 9 μm, a length between 100 and 300 μm with the density and aspect ratio of 1.75 $g{\cdot}cm^{-3}$ and 43, respectively [14]. Polyamide (PA) powder, grade PA 2200 (supplied by Sigma-Aldrich Sdn. Bhd., Malaysia) with a density of 0.45 $g{\cdot}cm^{-3}$ and tensile modulus and tensile strength of 1,620 and 48 MPa, respectively, was used as a binder. The compound materials were initially mixed at 20 wt% of CF and 80 wt% of PA with a mechanical mixer (KIKA RW20 WERK digital) at the rotational speed of 300 rpm for 4 min to mix homogenously [15]. Then, the compounded PACF with 10 mm cylinder length and 1 mm orifice diameter was prepared for rheology (Shimadzu CFT-500D) analysis. The rheological parameters varied from 210 to 250°C with the load cell between 40 and 80 N. Ultimaker S3 was used in printing samples using the FDM technique to prepare the PACF samples. The processing parameters were set at 250°C with the bed temperature, print speed, and layer height setting at 110°C, 80 $mm{\cdot}s^{-1}$, and 0.1 mm, respectively. The PACF samples were printed in different printing directions, namely, horizontal and vertical, with the dimensions of 124 mm × 12.7 mm × 3.2 mm based on ASTM D790. The samples eventually underwent the drying process at 70°C for 5 h and 20 h in a vacuum drying oven (Thermo Scientific Vacuum Oven 6000, Heraeus) to study the effects of the drying process on the interfacial adhesion and bonding.

2.2 Characterisation of PACF composites

The purity of PACF composites was analysed using an X-ray diffractometer (X-ray diffraction [XRD], Bruker AXS Germany, Model D8 Advance) at a range from 5° to 90° with CuKα (λ = 1.542 nm) beam and using Rietveld refinement (X'Pert HighScore Plus) software [15]. The thermal stability of PACF composites and its differential thermal analysis were determined using thermogravimetric analysis (TGA) and differential scanning calorimetry (DSC) using the Mettler Toledo machine. The temperature was between 30 and 900°C at 20 °C·min^{-1} temperature rate under nitrogen environment. The interfacial adhesion and bonding within the structural PACF composites were analysed using a scanning electron microscope (model Quanta FEI, Quanta 400F) and variable-pressure emission scanning electron microscopy (model Carl Zeiss Evo MA10). The composites were initially covered with gold coating using a sputter coater (model Polaron Quorum Q150R). The flexural strength of the printed PACF composite was examined using a universal testing machine (model Instron 5567, 30 kN) based on ASTM D790 with speed rate and support span set at 1 $mm{\cdot}min^{-1}$ and 72 mm, respectively. Also, the sample was tested at high temperature to check its reliability using universal testing machine (model Instron 5567, 30 kN) with round-line furnace based on ASTM D638-99 between 190 and 210°C at 5 $mm{\cdot}min^{-1}$ crosshead speed. Meanwhile, the shear test was conducted using 1 kN Instron 5567 with the use of epoxy adhesives (Loctite EA E-20HP Epoxy) cured for 24 h. The test was performed based on ASTM D5868-01 with its overlapping length of 25.4 mm. The epoxy thicknesses were maintained at an uniform rate of 0.06 mm before the shear test was performed at room temperature with 1.3 $mm{\cdot}min^{-1}$ crosshead displacement rate. As for the impact test, it was subjected to ASTM D5045-14 using 50J pendulum impact tester. The densification of the PACF composites was measured based on ASTM D792 using a standard level balance (Mettler Toledo, model ME-T Analytical Balance) with 0.998 $g{\cdot}cm^{-3}$ of distilled water.

3 Interlaminar shear behaviour of PACF composites

The influence of varying temperatures and drying times on the thermal behaviour of PACF composites is shown in thermograms in Figure 1a and b. Figure 1a exhibits that,

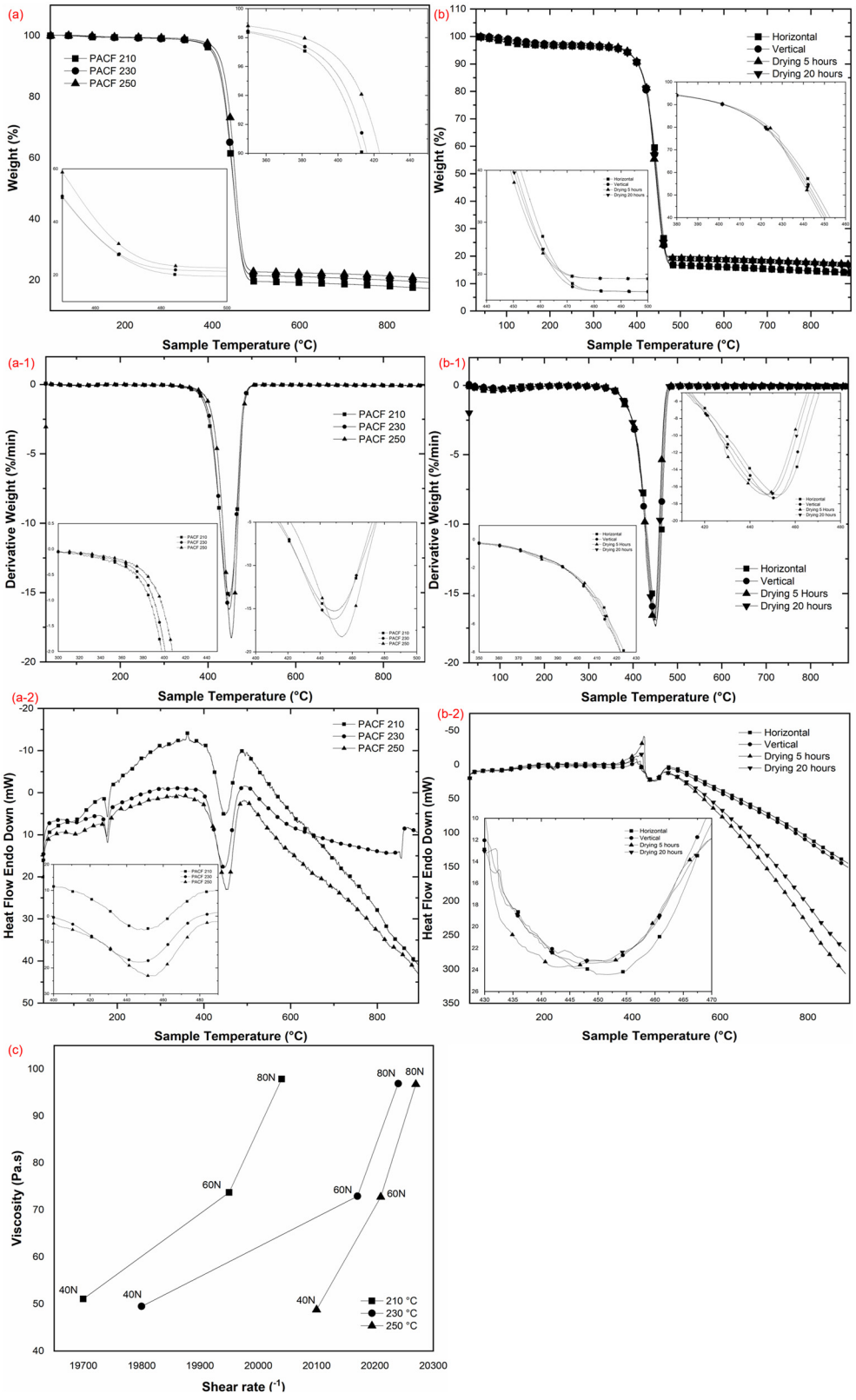

Figure 1: Thermal behaviour of PACF composites as recorded in (a) varying printing temperatures, (b) different printing directions and drying times. The derivative weight loss profile of PACF at (a-1) varying printing temperature and (b-1) vary printing directions and drying times. The DSC thermograph at (a-2) varying printing temperature and (b-2) vary printing directions and drying. The (c) rheological properties at temperature of 210°C, 230°C, and 250°C.

at 386°C, the thermal stability indicated a noticeable weight loss due to the solvent degradation, which then degraded to 498°C because of the polymer backbone degradation [16]. However, the thermograms in Figure 1b indicate that the thermal degradation experienced an early drop (~5% w/w) at 120°C because the PACF composites have been dried for several hours (between 5 and 20 h) [17]. These phenomena are attributed to a considerable loss of residual solvent; however, it can maintain its structural integrity longer than the PACF filament can (Figure 1a) [18]. Studies reported that this findings can be attributed to the onset degradation temperature (5% sample weight loss), which has a beneficial influence on the printed PACF thermal stability [19]. However, drastic changes were recorded (380–422°C) in the PACF filament (Figure 1a) compared to the printed PACF composites (Figure 1b). This observation indicated that the most consistent drop (380–455°C) in the printed PACF composites was attributed to high thermal boundary resistance [20]. Studies on nanocomposite materials showed that the low residual solvent contributes to the high contact within the filler, resulting in the gradual increase in filler networks and thermal conduction pathways [21]. However, Figure 1b indicates that the drying hours provided a minimum impact on the thermal behaviour as the materials were fabricated in the printed PACF structure. A slight difference (5% w/w) existsed in the third thermogram step between the undried printed PACF and the dried printed PACF composites (denoted as horizontal and vertical), as shown in Figure 1b. This behaviour was explained fully in studies on printed thermoplastic materials; these studies indicated that the heat applied during the drying process emitted the particles on the PACF itself [22]. Thus, a small amount of material was vaporised and transformed into particles during TGA at specific temperatures [19]. Printing composite materials often depend on volatile materials, particle concentration, and particle size, and they vary from conventionally produced composite materials [23]. The studies of printing composites indicated that the drying process shortens the polymer chain [19]. This phenomenon explained how different dried and undried printed PACFs behaved (Figure 1b), as given that drying consequently affected the interfacial strength during the printing process and the non-homogenous melt viscosity, and the materials did not dry up (longer polymer chains) [19].

Figure 1(a-1) and (b-1) clearly shows that the derivative weight loss profile has a single peak, which is related to carbon degradation at temperatures between 410 and 480°C [24]. The major weight loss caused by carbon combustion demonstrated good thermostability with the temperature set at 410°C [25,26]. Figure 1(a-1) shows that the scission of the imide group, which is caused by the gaseous oxidation of carbon, results in two-step degradations of PACF filament (PACF 250) [25]. The second minor degradation temperature would result in the carbon bonding breakage [27]. As shown in Figure 1b and (b-1), the PACF filament allows for an appropiate carbon growth range (410–450°C) as it undergoes the fabrication (additive manufacturing) process. These findings suggest that the PACF printed in a layer-by-layer sequence has good stability, as evidenced by studies using CFs and carbon nanotubes, which found similar growth ranges and stability upon fabrication [28]. The thermal stability of printed PACF is better that that of PACF filament; however, as shown in Figure 1(b-1), studies clearly indicated that the stability of the dried printed PACF is better than that of as-is printed PACF because the former has minimum loss in fibres [26,29]. The DSC thermograph shown in Figure 1(a-2) indicates that the filament composites encounter endothermic peaks at 180 and 445°C. In comparison, the printed PACF for both as-is and dried conditions encounters exothermic peaks at 455°C, as shown in Figure 1(b-2). The second endothermic peaks experienced by the PACF filament are obviously due to the inherent moisture content that was not entirely removed during the first endothermic cycle [30]. The studies by Radzuan et al. [30] indicated that the exothermic occurrence must be attributed to the moisture desorption, resulting in the immediate release. This observation shows that the dried-up condition (5 and 20 h) affected the interfacial bonding of the composite materials subjected to adhesion behaviour; thus, the heat resistance of the dried printed PACF materials is better than that of as-is printed PACF materials [31]. In 2020, a study on concrete 3D print highlighted that additional heating is a viable option prior to the stacking layup sequence [32].

The rheological behaviour was studied to enhance the adhesion and interfacial bonding during the printing process, particularly when customised compositions were considered, as shown in Figure 1c. Previous studies reported that rheological behaviour is crucial for increasing the bonding strength and interlocking stability and avoiding excessive deformation during the printing process [32]. On the contrary, shear-thickening characteristics appeared as the temperature increased from 210 to 250°C, as shown in Figure 1c. The shear induced the formation of the transient networks of particle suspensions because the polymer bridge is thought to cause these phenomena [33]. As reported in earlier investigations, a drastic shift in shear rates between 210 and 250°C indicates a strong network structure because the shear thickening is prominent [34].

The shear-thickening behaviour was caused by the limited amount of composition (20 wt% of CF) employed in filament fabrication. This phenomenon allows the polymer chain to expand via a large number of bridges during the polymer adsorption on a solid surface, resulting in shear thickening [35]. Yeh et al. [36] explained this phenomenon as a shear-thickening behaviour that occurs when the shear rate approaches a critical value, which is commonly observed in colloidal suspensions and polymer solutions. In a study on Kevlar composites, Yeh et al. [36] reported that adding layers to the composites cause shear-thickening effects, which aid in impact resistance. Studies on 3D printed materials showed that shear thickening is attributed to the hydrophilic PACF structure, which forms a stable network surface despite the bonding, demonstrating a high-viscosity non-Newtonian slurry [37]. Figure 2c shows that the maximum shear rate offset at 250°C, together with the highest shear-thickening behaviour, resulted in samples with a smooth surface compared to samples at 210 and 230°C (Figure 2a and b). This observation reveals that when heat is induced, the thickness of the absorbed layer is reduced (20–30 nm); this phenomenon is attributed to shear thickening [35]. However, it results in a smooth filament surface, which improves the interfacial adhesion and bonding throughout the printing process [38]. In 2018, research on carbon-based particles highlighted that adding carbon particles and particles with a large surface area can improve shear thickening and provide a wide range of functionality [39]. Thus, the geometrical shape of the filler should be considered when carbon (>20 wt%) is added because it affects the rheological characteristics and ensures a smooth printing process. In particular, shear thichkening allows for the layer printing of materials with a smooth surface while maintaining good adhesion within the printed layer [40]. Figure 2a demonstrates the clear micrograph images of the filaments with an uneven surface at 210°C, compared to those at 250°C in Figure 2c. A smooth surface ensures that the bonding within the printed layers possesses excellent interfacial adhesion, thereby avoiding the delamination occurrence, while the printed composites were cooled at room temperature [41].

Figure 3a shows the XRD characteristic peaks of PA and CF. The interlayer spacing and diffracting peaks of PACF composites were detected using XRD in several printing directions and drying times. These results were caused by the compositions of the PA (80%) and CF (20%) composites employed in this study. As shown in

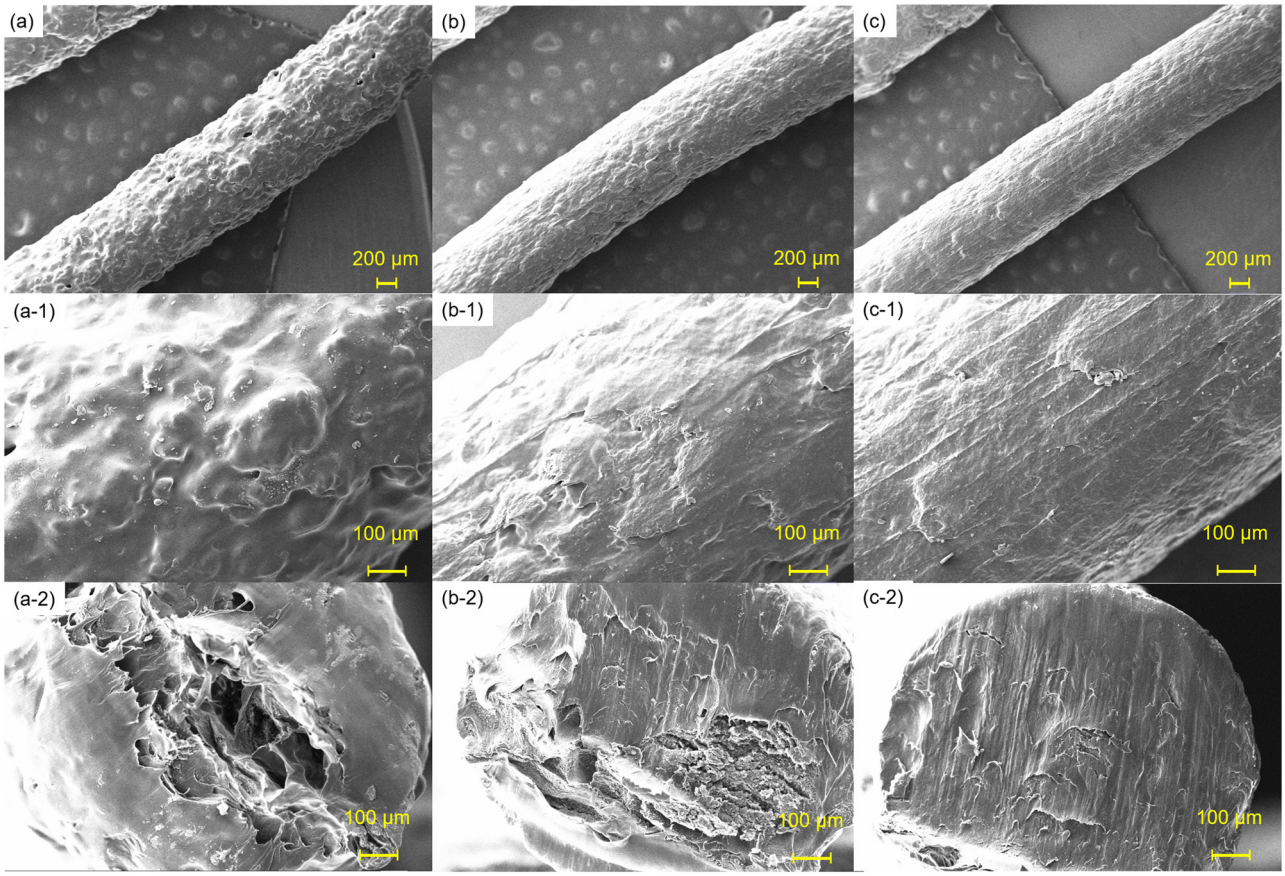

Figure 2: SEM pictures of PACF composite sample: (a) 210°C, (b) 230°C, and (c) 250°C.

Figure 3a of XRD diffractogram, all PACF specimens have distinctive diffracting peaks at 2θ = 23.36°, 22.71°, 20.34°, and 23.47°, which correspond to the vertical, horizontal, drying 5 h, and drying 20 h of samples. This peak became slightly intense as the printing direction changed from the vertical to the horizontal direction. However, a strong peak of the vertical direction sample at 23.36° revealed a difference in PACF *d*-spacing when the direction was changed to horizontal, increasing from 3.81 to approximately 3.91 nm. Many factors were investigated to determine which factors impacted the directional of the PACF sample. The processing temperature [42] and the bed temperature [43] were two external factors that affected the processing condition. In addition, the diffraction peaks that were dried for extended periods (20 h) exhibited a great peak at 23.47°, linked with the crystalline phase of PACF in the XRD patterns [44]. The possible reason is that a large energy input on the PACF powder caused considerable melting, and then other phases were generated from the melt during the subsequent crystallisation process [45].

4 Mechanical strength analysis relation with interlaminar shear behaviour

Composite materials with excellent mechanical properties are important in engineering application [46]. In this study, the printed sample of PACF composites was tested for flexural properties as a function of different printing directions and drying times. During the flexural test, both directions of the PACF sample undergo bending upon the applied load with a delamination toward the sides of the sample, as shown in Figure 3b. This delamination in the PACF sample was caused by poor interfacial adhesion between the adjacent layers that represent a load transfer between the matrix (PA) and the CFs [47]. During the test, when the PACF sample underwent bending upon the applied load, the flexural strength and modulus of the horizontal direction sample were higher than those of the vertical sample at 52.90 MPa and 1.77 GPa, respectively, because the horizontal sample exhibited a high interfacial bonding between the PACF printed composites layers [9]. Figure 3b shows that a drastic deterioration in the vertical sample was observed in flexural strength and modulus (23.07 MPa and 0.56 GPa) because of improper interlocking between the fibre and matrix during the printing process [48]. This interlocking between the fibres at the vertical direction exhibited a weak formation of mechanical interlocking when compared to that at the horizontal direction of the PACF sample [49]. In addition, a considerable difference existed between the horizontal and vertical samples because of the constraints for the elongation of fibre threads along the sample, resulting in fibres with a high bending load capacity at the horizontal direction [50].

The horizontal sample was set at 70°C temperature in a vacuum drying oven to increase the bond strength of the PACF composites by performing a drying process for 5

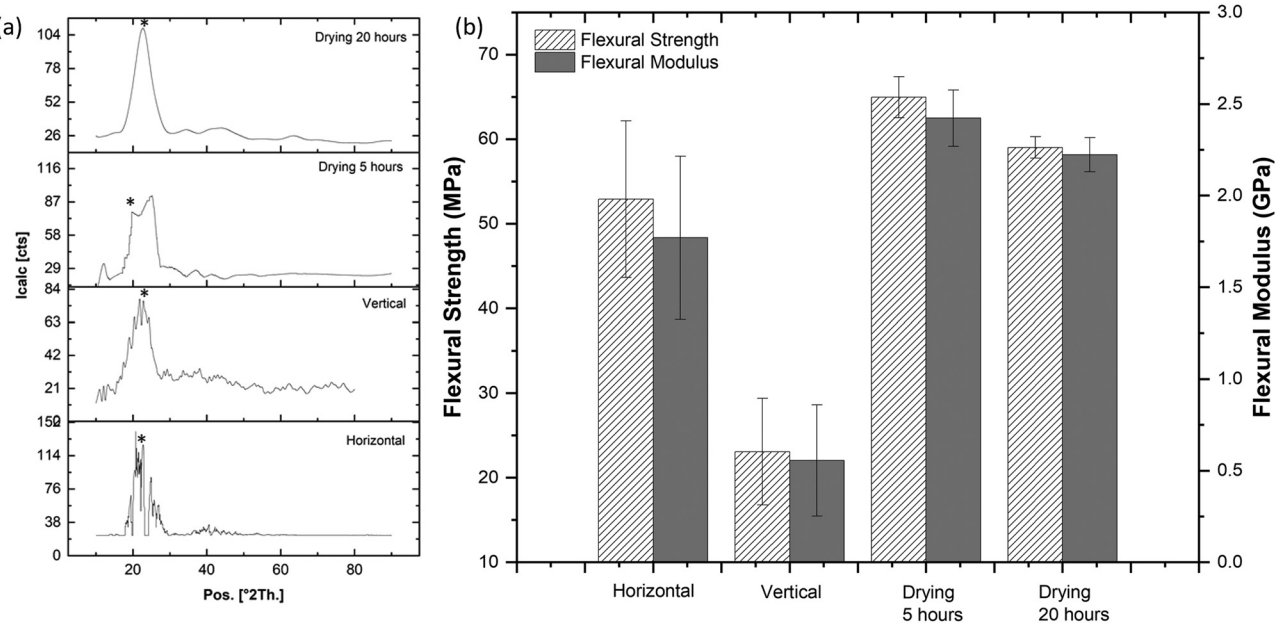

Figure 3: (a) XRD crystallography of PACF sample printed in various directions and drying for various hours and (b) flexural bending test on PACF composites.

and 20 h for the solidification between layers in PACF composites. The PACF samples were assessed with another flexural test after both horizontal directions were dried in the oven to observe whether the drying process affected the strength of the composites in the PACF samples. As shown in Figure 3b, the horizontal direction of the printed PACF dried for 5 h exhibited the highest flexural strength and modulus with 64.95 MPa and 2.42 GPa, respectively, allowing the formation of a solid structure of composites [51]. When the PACF sample was dried for 20 h, the flexural strength and modulus dropped to 59.007 MPa and 2.223 GPa, respectively. This scenario indicates a decrease in the molecular weight of the polymer matrix, making the PACF sample to be slightly stiff. This phenomenon showed that during the drying process of PACF composites (fibre breakdown), the ability to restrict the polymer composite chain mobility decreased because of the drop in the molecular weight of the PACF sample. As this research aims to study the interfacial bonding of the PACF composites, the effects of voids within the CF on the flexural behaviour are considered.

The mechanical properties acquired in this study were evaluated in scanning electron microscopy (SEM) to assess the performance of the printed composites. Fracture interface observations after flexural testing were used to investigate these phenomena, as illustrated in Figure 4. According to SEM observations, the air void in the interfacial zone of the horizontal direction was larger than that in the vertical direction of the sample. The empty parts in the horizontal printed sample were left as voids because the fibre area was unfilled with PA matrix. In addition, the mechanical performance of the horizontal printed sample weakens because of the non-uniform dispersion of the fibre [13]. The effect of void content is frequently stated in the literature as a reduction in flexural strength proportionate to the high void content [52]. However, in this scenario, the flexural strength of the horizontal sample was higher than that of the vertical sample. Thus, the outcome was the opposite when the horizontal sample had a larger void content than the vertical sample. The building direction had an impact on the vertically printed PACF composites (with less void) under these conditions.

Meanwhile, the obtained microstructural features of the region covered with PA at a printing speed of 80 $mm \cdot s^{-1}$ in the vertical direction were recorded as shown in Figure 4. Figure 4 shows the cross-sectional morphologies of PACF created in a horizontal direction at a specified period using a 70°C drying temperature. After the sample was dried, the SEM of the flexural testing revealed that both of the PACF samples had identified the damage and the function of voids [52]. The interfacial bonding and binding forces between the two printed samples explain the acquired results on the drying sample at different times [51].

In accordance with the flexural strength test, horizontal printed direction with the drying of 5 h was later printed in the form of impact and shear test samples. Results in Figure 5a clearly indicate that the maximum absorbed impact energy was recorded at 4.8 J, while the average was recorded at 4.3 J. Meanwhile, the maximum impact strength of 38 $kJ \cdot m^{-2}$ shown in Figure 5b is way above the present study reported by Rahmanian et al. [53]. They reported that their carbon-based materials which were fabricated by conventional casting are

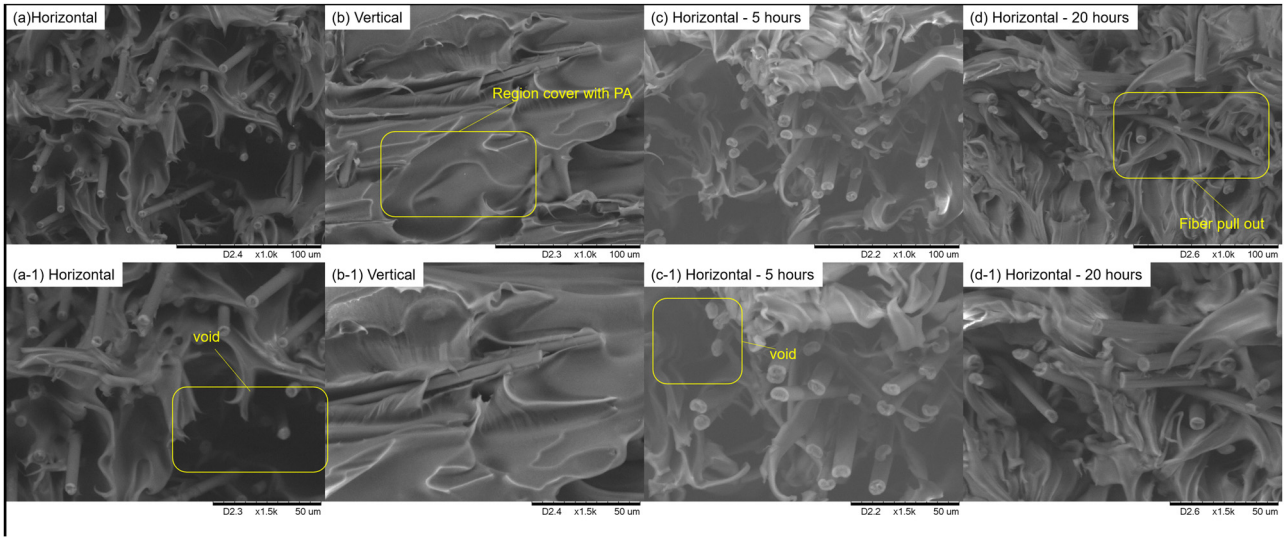

Figure 4: SEM (×1,000) and (×1,500) of PACF composites: direction of (a) horizontal and (b) vertical; dried for (c) 5 h and (d) 20 h.

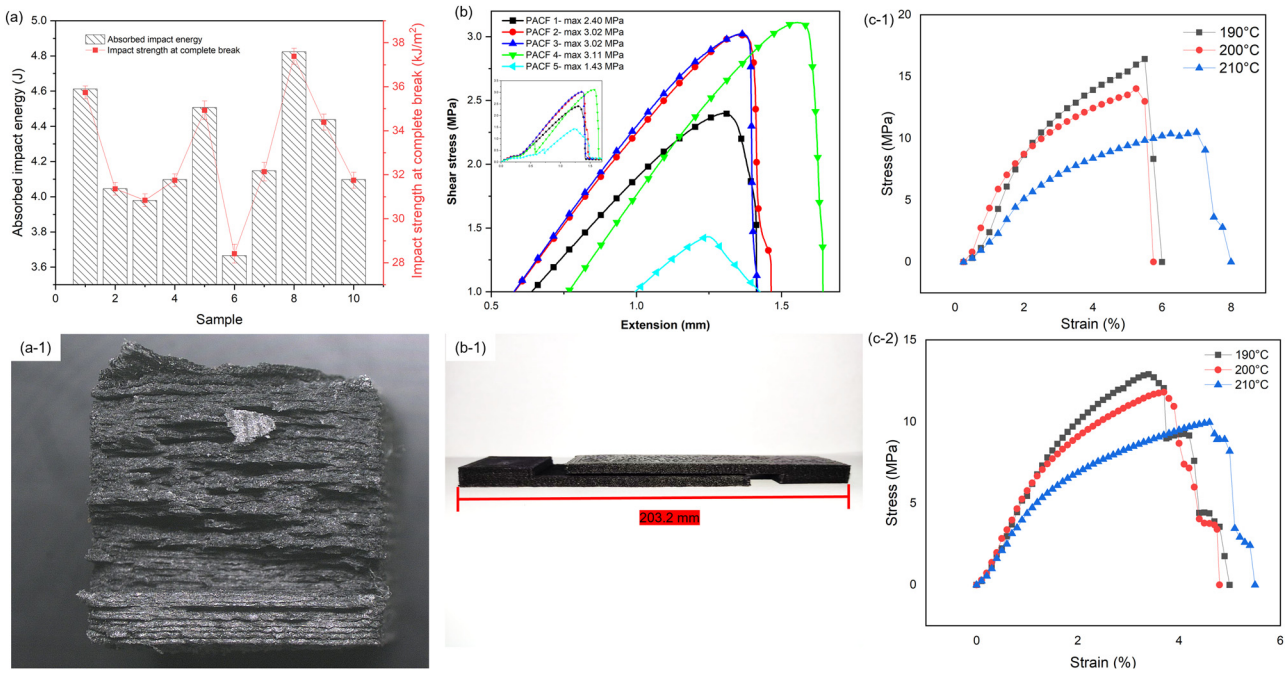

Figure 5: Mechanical strength of printed PACF: (a) impact strength with (a-1) micrograph image of fracture sample view, (b) shear strength, (b-1) shear test sample dimension, and tensile test between 190 and 210°C for (c-1) 5 h and (c-2) 20 h.

between 0.5 and 3 kJ·m^{-2}. In fact, this study also improved its impact strength by 240% as compared to pure PA that earlier recorded an average of 15.9 kJ·m^{-2} [54]. Notably, the absorbed impact energy is low compared to the pure PA ranging between 80 and 140 J due to the CF addition. This are due to the fact that since the pure polymer or elastic body, the amount of impact energy is spent in terms of elastic deformation. However, the reported data in this study are considerably high compared to laminate carbon–epoxy materials, which exhibited absorbed energy ranging between 0 and 2.5 J [55]. These clearly indicated that the energy absorbed by the horizontally printed PACF most likely depend on the interfaces between the differently oriented layers as shown in Figure 5(a-1). Similar trends were reported by Quaresimin et al. [55] as they studied the laminated layers and indicated that the damage occurred upon the impact strength caused by the delamination mainly developed within the interfaces. Although sample no. 6 in Figure 5a experienced sudden drop of absorbed impact energy and impact strength at 3.6 J and 28 kJ·m^{-2}, respectively, Murray et al. [56] reported that this observation was random from this specific sample and not common for the sample set.

While for shear strength the printed samples recorded a maximum of 3.11 MPa and lowest of 1.43 MPa (Figure 5b). This indicated that there are evidence of stable segregation between the layups interfacial especially for sample numbers 2, 3, and 4. Meanwhile, the lowest 1.43 MPa recorded suggested that the samples fail due to the imperfections or misalignments during printing processes as reported by Yap et al. [57]. The results obtained were dramatically low when compared to the flexural strength recorded between 45 and 70 MPa. Yap et al. [57] reported that the huge loop were subjected to the adherend experienced by the shear test samples as the fracture occurrence is in the epoxy resin regions. Hence, it caused the single lap shear samples to experience low shear strength (average of 3 MPa). However, contradict results were obtained by Chen et al. [58] as they investigated the interlaminar shear strength of PA composites using flexural strength. They discovered a similar trend between 60 and 70 MPa (flexural strength) caused by the interfacial bonding within matrix and fillers that improved the de-blocking behaviour as more isocyanate groups were generated. These further enhance the bond formation occurrences linked to surface interface which is also reported in conventional process [59].

To ensure its mechanical performance at high temperature, the tensile test was performed at temperature between 190 and 210°C. Figure 5(c-1) clearly recorded that the tensile strength for 5 h drying time is 33% higher compared to 20 h drying time shown in Figure 5(c-2). Since these phenomena were at higher drying time, the interface between the printed PACF tends to deteriorate which is proven as shown in Figure 4. Meanwhile, Figure 5(c-1) and (c-2)

indicates a strength decrease as the temperature rises. Tholibon et al. [60] in their study mentioned that this behaviour was related to the thermal decomposition of the fibre and the PA, which tends to degrade as the temperature increases to 210°C. However, the tensile strength performance of printed PACF was 800% higher compared to PA-6-reinforced CF at 280°C recorded at ~2 MPa when prepared using thermoforming technique [61]. These exhibited that while controlling the printing parameters the drying process will improve the mechanical performance in comparison with conventional fabrication process.

5 Conclusion

The usage of PACF as a material for increasing the mechanical characteristics of composites has been proven effective as its ability to enhance the bonding between the layers while increasing the interfacial adhesion by controlling the filament printable directions and drying process. The use of 20 wt% CF as reinforcement enhanced the printing direction of the fibre, influencing the flexural strength. According to SEM, the presence of voids left in the printed samples was influenced by the printing direction. As a result of the additional treatment with the 5 h drying process, the interfacial adhesion between PA and CF increased by 23%. This 20 wt% PACF with 5 h drying time was able to increase its impact test by 240% when compared to pure PA. However, the shear strength test was low (~3 MPa) subjected to the epoxy resin adjoint during the shear test; meanwhile, the impact test indicated 29% difference in the overall recorded data. Hence, further considerations will include the increase of filament contents (>20 wt%) to broaden its conductive polymeric applications.

Acknowledgements: The authors wish to thank and acknowledge the Ministry of Higher Education (MOHE) and the Centre for Research and Instrumentation Management (CRIM), Universiti Kebangsaan Malaysia, for their financial support to complete this study under grant number FRGS/1/2020/TK0/UKM/02/18. The authors would also like to thank Final Year Project's students Mohammad Ashraf Bin Mohammad Amin and Muhamad Nasrul Bin Ridzuan for their contribution in experimental validation.

Funding information: Ministry of Higher Education (MOHE) and the Centre for Research and Instrumentation Management (CRIM), Universiti Kebangsaan Malaysia, for their financial support to complete this study under grant number FRGS/1/2020/TK0/UKM/02/18.

Author contributions: Nisa Naima Khalid: investigation and data analysis; Nabilah Afiqah Mohd Radzuan: writing, editing, conceptualisation, methodology, validation, supervision, and funding acquisition; Abu Bakar Sulong: supervision; David Hui: supervision; Farhana Foudzi: supervision.

Conflict of interest: One of the coauthors serves as an Editor in Chief in the journal.

References

[1] Friedrich, K. and A. A. Almajid. Manufacturing aspects of advanced polymer composites for automotive applications. *Applied Composite Materials*, Vol. 20, No. 2, 2013, pp. 107–128.

[2] Gao, X., N. Yu, and J. Li. Influence of printing parameters and filament quality on structure and properties of polymer composite components used in the fields of automotive. *Structure and Properties of Additive Manufactured Polymer Components*, 2020, pp. 303–330.

[3] Liu, Z., Q. Lei, and S. Xing. Mechanical characteristics of wood, ceramic, metal and carbon fiber-based PLA composites fabricated by FDM. *Journal of Materials Research and Technology*, Vol. 8, No. 5, 2019, pp. 3743–3753.

[4] Penumakala, P. K., J. Santo, and A. Thomas. A critical review on the fused deposition modeling of thermoplastic polymer composites. *Composites Part B: Engineering*, Vol. 201, 2020, id. 108336.

[5] Davim, J. P., Ed. Green composites. Materials, Manufacturing and Engineering. *Advanced Composites*, De Gruyter, Vol. 7, pp. 1–149, 2017.

[6] Bilkar, D., R. Keshavamurthy, and V. Tambrallimath. Influence of carbon nanofiber reinforcement on mechanical properties of polymer composites developed by FDM. *Materials Today: Proceedings*, Vol. 46, 2021, pp. 4559–4562.

[7] Peng, X., M. Zhang, Z. Guo, L. Sang, and W. Hou. Investigation of processing parameters on tensile performance for FDM-printed carbon fiber reinforced polyamide 6 composites. *Composites Communications*, Vol. 22, 2020, id. 100478.

[8] Ngo, T. D., A. Kashani, G. Imbalzano, K. T. Q. Nguyen, and D. Hui. Additive manufacturing (3D printing): a review of materials, methods, applications and challenges. *Composites Part B: Engineering*, Vol. 143, 2017, 2018, pp. 172–196.

[9] Maqsood, N. and M. Rimašauskas. Delamination observation occurred during the flexural bending in additively manufactured PLA-short carbon fiber filament reinforced with continuous carbon fiber composite. *Results in Engineering*, Vol. 11, 2021, id. 100246.

[10] Dave, H. K. and J. P. Davim, Eds., *Fused deposition modeling based 3D printing*. Springer International Publishing, Cham, 2021.

[11] Ota, H., S. Emaminejad, Y. Gao, A. Zhao, E. Wu, S. Challa, et al. Application of 3D printing for smart objects with embedded

electronic sensors and systems. *Advanced Materials Technologies*, Vol. 1, No. 1, 2016, id. 1600013.
[12] Behera, D., S. Chizari, L. A. Shaw, M. Porter, R. Hensleigh, Z. Xu, et al. Current challenges and potential directions towards precision microscale additive manufacturing – Part IV: future perspectives. *Precision Engineering*, Vol. 68, 2021, pp. 197–205.
[13] Wickramasinghe, S., T. Do, and P. Tran. FDM-based 3D printing of polymer and associated composite: a review on mechanical properties, defects and treatments. *Polymers*, Vol. 12, No. 7, 2020, pp. 1–42.
[14] Mohd Radzuan, N. A., A. B. Sulong, M. R. Somalu, A. T. Abdullah, T. Husaini, R. E. Rosli, et al. Fibre orientation effect on polypropylene/milled carbon fiber composites in the presence of carbon nanotubes or graphene as a secondary filler: application on PEM fuel cell bipolar plate. *International Journal of Hydrogen Energy*, Vol. 44, No. 58, 2019, pp. 30618–30626.
[15] Radzuan, N. A. M., A. B. Sulong, M. Irwan, M. Firdaus, T. Husaini, and E. H. Majlan. Fabrication of multi-filler MCF/MWCNT/SG-based bipolar plates. *Ceramics International*, Vol. 45, No. 6, 2019, pp. 7413–7418.
[16] Krathumkhet, N., K. Vongjitpimol, T. Chuesutham, S. Changkhamchom, K. Phasuksom, A. Sirivat, et al. Preparation of sulfonated zeolite ZSM-5/sulfonated polysulfone composite membranes as PEM for direct methanol fuel cell application. *Solid State Ionics*, Vol. 319, August 2017, 2018, pp. 278–284.
[17] Wang, Y., H. Wan, D. Wang, J. Wang, L. Wang, and R. Feng. Preparation and characterization of a semi-interpenetrating network alkaline anion exchange membrane. *Fibers and Polymers*, Vol. 19, No. 1, 2018, pp. 11–21.
[18] Lee, H. J., M. K. Cho, Y. Y. Jo, K. S. Lee, H. J. Kim, E. Cho, et al. Application of TGA techniques to analyze the compositional and structural degradation of PEMFC MEAs. *Polymer Degradation and Stability*, Vol. 97, No. 6, 2012, pp. 1010–1016.
[19] Vidakis, N., M. Petousis, L. Tzounis, S. A. Grammatikos, E. Porfyrakis, A. Maniadi, et al. Sustainable additive manufacturing: mechanical response of polyethylene terephthalate glycol over multiple recycling processes. *Materials*, Vol. 14, No. 5, 2021, id. 1162.
[20] Wang, J., J. J. Li, G. J. Weng, and Y. Su. The effects of temperature and alignment state of nanofillers on the thermal conductivity of both metal and nonmetal based graphene nanocomposites. *Acta Materialia*, Vol. 185, 2020, pp. 461–473.
[21] Li, J., P. Zhang, H. He, and B. Shi. Enhanced the thermal conductivity of flexible copper foil by introducing graphene. *Materials and Design*, Vol. 187, 2020, id. 108373.
[22] Sittichompoo, S., S. Kanagalingam, L. E. J. Thomas-Seale, A. Tsolakis, and J. M. Herreros. Characterization of particle emission from thermoplastic additive manufacturing. *Atmospheric Environment*, Vol. 239, 2020, id. 117765.
[23] Evgin, T., A. Turgut, G. Hamaoui, Z. Spitalsky, N. Horny, M. Micusik, et al. Size effects of graphene nanoplatelets on the properties of high-density polyethylene nanocomposites: morphological, thermal, electrical, and mechanical characterization. *Beilstein Journal of Nanotechnology*, Vol. 11, 2020, pp. 167–179.
[24] Morales Ibarra, R., M. Sasaki, M. Goto, A. T. Quitain, S. M. García Montes, and J. A. Aguilar-Garib. Carbon fiber recovery using water and benzyl alcohol in subcritical and supercritical conditions for chemical recycling of thermoset composite materials. *Journal of Material Cycles and Waste Management*, Vol. 17, No. 2, 2015, pp. 369–379.
[25] Sawangphruk, M., A. Krittayavathananon, and N. Chinwipas. Ultraporous palladium on flexible graphene-coated carbon fiber paper as high-performance electro-catalysts for the electro-oxidation of ethanol. *Journal of Materials Chemistry A*, Vol. 1, No. 4, 2013, pp. 1030–1034.
[26] Batista, N. L., M. L. Costa, K. Iha, and E. C. Botelho. Thermal degradation and lifetime estimation of poly(ether imide)/carbon fiber composites. *Journal of Thermoplastic Composite Materials*, Vol. 28, No. 2, 2015, pp. 265–274.
[27] Seydibeyoğlu, M. Ö. A novel partially biobased PAN-lignin blend as a potential carbon fiber precursor. *Journal of Biomedicine and Biotechnology*, Vol. 2012, 2012, pp. 1–8.
[28] Zhang, Q., J. Liu, R. Sager, L. Dai, and J. Baur. Hierarchical composites of carbon nanotubes on carbon fiber: influence of growth condition on fiber tensile properties. *Composites Science and Technology*, Vol. 69, No. 5, 2009, pp. 594–601.
[29] Singha, A. S. and V. K. Thakur. Mechanical properties of natural fibre reinforced polymer composites. *Bulletin of Materials Science*, Vol. 31, No. 5, 2008, pp. 791–799.
[30] Radzuan, N. A. M., A. B. Sulong, T. Husaini, E. H. Majlan, M. I. Rosli, and M. F. Aman. Fabrication of multi-filler MCF/MWCNT/SG-based bipolar plates. *Ceramics International*, Vol. 45, No. 6, 2019, pp. 7413–7418.
[31] Han, P., A. Tofangchi, A. Deshpande, S. Zhang, and K. Hsu. An approach to improve interface healing in FFF-3D printed Ultem 1010 using laser pre-deposition heating. *Procedia Manufacturing*, Vol. 34, 2019, pp. 672–677.
[32] Muthukrishnan, S., S. Ramakrishnan, and J. Sanjayan. Effect of microwave heating on interlayer bonding and buildability of geopolymer 3D concrete printing. *Construction and Building Materials*, Vol. 265, 2020, id. 120786.
[33] Khandavalli, S. and J. P. Rothstein. Extensional rheology of shear-thickening fumed silica nanoparticles dispersed in an aqueous polyethylene oxide solution. *Journal of Rheology*, Vol. 58, No. 2, 2014, pp. 411–431.
[34] Zhang, S., S. Wang, Y. Wang, X. Fan, L. Ding, S. Xuan, et al. Conductive shear thickening gel/polyurethane sponge: a flexible human motion detection sensor with excellent safeguarding performance. *Composites Part A: Applied Science and Manufacturing*, Vol. 112, 2018, pp. 197–206.
[35] Kamibayashi, M., H. Ogura, and Y. Otsubo. Shear-thickening flow of nanoparticle suspensions flocculated by polymer bridging. *Journal of Colloid and Interface Science*, Vol. 321, No. 2, 2008, pp. 294–301.
[36] Yeh, S. K., J. J. Lin, H. Y. Zhuang, Y. C. Chen, H. C. Chang, J. Y. Zheng, et al. Light shear thickening fluid (STF)/Kevlar composites with improved ballistic impact strength. *Journal of Polymer Research*, Vol. 26, No. 6, 2019, id. 155.
[37] Cai, P., L. Guo, H. Wang, J. Li, J. Li, Y. Qiu, et al. Effects of slurry mixing methods and solid loading on 3D printed silica glass parts based on DLP stereolithography. *Ceramics International*, Vol. 46, No. 10, 2020, pp. 16833–16841.
[38] Valino, A. D., J. R. C. Dizon, A. H. Espera, Q. Chen, J. Messman, and R. C. Advincula. Advances in 3D printing of thermoplastic polymer composites and nanocomposites. *Progress in Polymer Science*, Vol. 98, 2019, id. 101162.

[39] Jeong, H. T., J. Kim, and T. J. Kang. Control of shear thickening onsets by nanoparticles. *Fibers and Polymers*, Vol. 19, No. 5, 2018, pp. 997–1003.
[40] Ji, H., X. Zhang, X. Huang, L. Zheng, X. Ye, and Y. Li. Effect of extrusion on viscoelastic slurry 3D print quality: numerical analysis and experiment validation. *SN Applied Sciences*, Vol. 1, No. 9, 2019, id. 1036.
[41] Stark, M. S. Improving and understanding inter-filament bonding in 3D-printed polymers. University of Tennessee Honors Thesis Project, Chancellor's Honors Program Projects. 2016, pp. 1–25. https://trace.tennessee.edu/utk_chanhonoproj/1997.
[42] Arefin, A. M. E., N. R. Khatri, N. Kulkarni, and P. F. Egan. Polymer 3D printing review: materials, process, and design strategies for medical applications. *Polymers*, Vol. 13, No. 9. 2021, pp. 1499.
[43] Choi, Y.-H., C.-M. Kim, H.-S. Jeong, and J.-H. Youn. Influence of bed temperature on heat shrinkage shape error in FDM additive manufacturing of the ABS-engineering plastic. *World Journal of Engineering and Technology*, Vol. 04, No. 03, 2016, pp. 186–192.
[44] Chen, P., H. Wu, W. Zhu, L. Yang, Z. Li, C. Yan, et al. Investigation into the processability, recyclability and crystalline structure of selective laser sintered polyamide 6 in comparison with polyamide 12. *Polymer Testing*, Vol. 69, 2018, pp. 366–374.
[45] Zhu, W., C. Yan, Y. Shi, S. Wen, J. Liu, and Y. Shi. Investigation into mechanical and microstructural properties of polypropylene manufactured by selective laser sintering in comparison with injection molding counterparts. *Materials and Design*, Vol. 82, 2015, pp. 37–45.
[46] Srivastava, M. and S. Rathee. Optimisation of FDM process parameters by Taguchi method for imparting customised properties to components. *Virtual and Physical Prototyping*, Vol. 13, No. 3, 2018, pp. 203–210.
[47] Polyzos, E., A. Katalagarianakis, D. Van Hemelrijck, and L. Pyl. Delamination analysis of 3D-printed nylon reinforced with continuous carbon fibers. *Additive Manufacturing*, Vol. 46, April, 2021, id. 102144.
[48] Ravichandiran, N., C. Kannan, R. Senthil, and R. L Gopinathan. National conference on recent trends and developments in sustainable green technologies design and analysis of drag and lift vertical axis national conference on recent trends and developments in sustainable green technologies. *Jchps*, Vol. 7, 2015, pp. 78–81.
[49] Lee, M. C., S. C. Koay, M. Y. Chan, H. L. Choo, M. M. Pang, P. M. Chou, et al. Properties of poly(lactic acid)/durian husk fiber biocomposites: effects of fiber content and processing aid. *Journal of Thermoplastic Composite Materials*, Vol. 33, No. 11, 2020, pp. 1518–1532.
[50] Alavudeen, A., N. Rajini, S. Karthikeyan, M. Thiruchitrambalam, and N. Venkateshwaren. mechanical properties of banana/kenaf fiber-reinforced hybrid polyester composites: effect of woven fabric and random orientation. *Materials & Design*, Vol. 66, 2015, pp. 246–257.
[51] Slavcheva, G. S. Drying and shrinkage of cement paste for 3D printable concrete. *IOP Conference Series: Materials Science and Engineering*, Vol. 481, No. 1, 2019, id. 012043.
[52] Suhot, M. A. and A. R. Chambers. The effects of voids on the flexural properties and failure mechanisms of carbon/epoxy composites. *Jurnal Teknologi*, Vol. 71, No. 2, 2014, id. 3736.
[53] Rahmanian, S., A. R. Suraya, M. A. Shazed, R. Zahari, and E. S. Zainudin. Mechanical characterization of epoxy composite with multiscale reinforcements: carbon nanotubes and short carbon fibers. *Materials and Design*, Vol. 60, 2014, pp. 34–40.
[54] Odrobina, M., T. Deák, L. Székely, T. Mankovits, R. Z. Keresztes, and G. Kalácska. The effect of crystallinity on the toughness of cast polyamide 6 rods with different diameters. *Polymers*, Vol. 12, No. 2, 2020, pp. 293.
[55] Quaresimin, M., M. Ricotta, L. Martello, and S. Mian. Energy absorption in composite laminates under impact loading. *Composites Part B: Engineering*, Vol. 44, No. 1, 2013, pp. 133–140.
[56] Murray, J. J., T. Allen, S. Bickerton, A. Bajpai, K. Gleich, E. D. McCarthy, et al. Thermoplastic RTM: impact properties of anionically polymerised polyamide 6 composites for structural automotive parts. *Energies*, Vol. 14, No. 18, 2021, id. 5790.
[57] Yap, Y. L., W. Toh, R. Koneru, R. Lin, K. I. Chan, H. Guang, et al. Evaluation of structural epoxy and cyanoacrylate adhesives on jointed 3D printed polymeric materials. *International Journal of Adhesion and Adhesives*, Vol. 100, 2020, id. 102602.
[58] Chen, K., M. Jia, H. Sun, and P. Xue. Thermoplastic reaction injection pultrusion for continuous glass fiber-reinforced polyamide-6 composites. *Materials*, Vol. 12, No. 3, 2019, id. 463.
[59] Arun Prakash, V. R. and R. Viswanthan. Fabrication and characterization of echinoidea spike particles and kenaf natural fibre-reinforced azadirachta-indica blended epoxy multi-hybrid bio composite. *Composites Part A*, Vol. 118, 2019, pp. 317–326.
[60] Tholibon, D., A. B. Sulong, N. Muhammad, N. F. Ismail, I. Tharazi, and M. K. F. Md Radzi. Tensile properties of unidirectional kenaf fiber polypropylene composite. *Jurnal Teknologi*, Vol. 78, No. 6–9, 2016, pp. 101–106.
[61] Margossian, A., S. Bel, and R. Hinterhoelzl. On the characterisation of transverse tensile properties of molten unidirectional thermoplastic composite tapes for thermoforming simulations. *Composites Part A: Applied Science and Manufacturing*, Vol. 88, 2016, pp. 48–58.